Design principles for central pattern generators with preset rhythms

Matteo Lodi, Andrey L. Shilnikov, and Marco Storace, *Senior Member, IEEE*

***Abstract*—This paper is concerned with the design of synthetic central pattern generators (CPGs). Biological CPGs are neural circuits that determine a variety of rhythmic activities, including locomotion, in animals. A synthetic CPG is a network of dynamical elements (here called cells) properly coupled by various synapses to emulate rhythms produced by a biological CPG. We focus on CPGs for locomotion of quadrupeds and present our design approach, based on the principles of nonlinear dynamics, bifurcation theory and parameter optimization. This approach lets us to design the synthetic CPG with a set of desired rhythms and to switch between them as the parameter representing the control actions from the brain is varied. The developed 4-cell CPG can produce four distinct gaits: walk, trot, gallop, and bound, similar to the mouse locomotion. The robustness and adaptability of the network design principles are verified using different cell and synapse models.**

***Index Terms*—central pattern generators, neuronal models, bifurcation analysis, parameter optimization.**

I. Introduction

CENTRAL pattern generators (CPGs) for locomotion are [small] neural networks able to produce rhythmic outputs even in the absence of sensory feedback or higher motor planning centers inputs [1]–[4]. CPGs are studied at the crossroad between many diverse disciplines including biology, neuroscience, robotics, nonlinear dynamics, biomechanics, to name a few. Each discipline deals with this common topic using different tools and by pursuing different goals: knowing their physiological structure, understanding their functional roles, reproducing their functional mechanisms in developed mathematical models, or exploiting them in robotics or neuroprosthetics applications. Biological CPGs of most vertebrates are composed of a large number of coupled neurons, which can be subdivided into smaller clusters or cohorts that behave coherently. Therefore, the orchestrated activity of each cluster can be modeled as if it was produced by a single neuron. Such a cluster is termed in many ways: a neural population, a unit, a building block, or a *cell* – the term that we adopt in this paper. The cells are connected by synapses to create the CPG.

M. Lodi and M. Storace are with the Department of Electrical, Electronic, Telecommunications Engineering and Naval Architecture, University of Genoa, Via Opera Pia 11a, I-16145, Genova, Italy. A. Shilnikov is with the Neuroscience Institute and Department of Mathematics & Statistics, Georgia State University, 100 Piedmont Ave., Atlanta, GA 30303, USA. E-mail: marco.storace@unige.it. This work was partially supported by the University of Genoa. A.L.S. acknowledges that this work was partially funded by NSF grant IOS-1455527, RSF grant 14-41-00044 at the Lobachevsky University of Nizhny Novgorod, RFFI grant 11-01-00001, and MESRF project 14.740.11.0919, and thanks GSU Brain and Behaviors Initiative for the fellowship and pilot grant support.

Our approach to model motor CPGs is based on the theory of dynamical systems [5], [6], which is well suited for understanding a multiplicity of nonlinear recurrent oscillations, their stability conditions and bifurcations that can occur in such small rhythm-generating neural networks [7]–[10]. In this paper, we focus on models of CPGs that determine and control the locomotion of quadrupeds. In particular, we discuss a set of operating principles that are employed in our design of synthetic CPGs to reproduce a number of prescribed gaits specific for the mouse locomotion. Our goal is to derive design rules for the multi-functional CPGs that can produce distinct mouse gaits and smooth transitions between them, depending on some drive or bifurcation parameter. Such a parameter can represent a control action from the brain or, more precisely, the brainstem control throughout neurons acting as key intermediaries between higher motor planning centers and the projected CPGs [11]–[13]. Previously, we proposed the computational toolkit CEPAGE [15] to analyze dynamics and bifurcations in simple CPGs emulating quadruped (mouse) locomotion as the control parameter is varied [14], [16]. Here we present an advanced 4-cell CPG model that more phenomenologically fits biological CPGs governing quadruped locomotion, being able to generate four different gaits: walk, trot, gallop and bound. We also discuss minimal operating principles as well as generic properties the adopted models of cells and synapses should meet to ensure the robustness and structural stability of the desired CPG functions.

In summary, in this paper we: (i) point out the qualitative properties that the cell and synapse models must be endowed with to meet the design goals; (ii) define a sequence of steps to design a reduced multifunctional CPG model producing several rhythms and switch between them smoothly with variations of the control parameter; (iii) demonstrate that our design approach is quite robust with respect to the choice of synapse and cell models.

The rest of this paper is organized as follows. Section II introduces the main features of the developed CPG. Section III presents in detail the proposed know-how to design a synthetic CPG with preset rhythms. In Section IV we verify the robustness of the proposed design with respect to changes in its components (models). Finally, Section V draws some conclusions.

II. Basic elements

In this section we summarize the pivotal elements of the proposed CPG design approach.

A. Cell

Our primary goal is better understanding the *functional* mechanisms underlying rhythmogenesis in biological CPGs. Therefore, our description of any cell in this paper is not meant to provide a 1:1 correspondence to a synchronous group of neurons, but rather a macro-model for several groups of interneurons functioning together, like half-center oscillators, for example. In other words, our CPG models have a level of abstraction higher than usual. In this perspective, the hierarchical structures often adopted to represent CPGs [17] or the functional subnetwork approach proposed in [18] can be hardly compared to our neural circuits as the CPGs designed according to the former approaches have a finer granularity, i.e., they contain a larger number of cells than our reduced models. The activity of the generic i-th cell is revealed through a variable representing its membrane voltage $V_i(t)$.

B. Phenomenological design outline

Rhythmic movements in animals result from the interplay between the sensory system (sensor), the musculoskeletal system (actuator), and the neural system (control). The neural system, in particular, performs three main control actions [3]. The first, open-loop control action is provided at the level of the spinal cord by the CPG generating the given pace; these neural networks include half-center oscillators – a pair of neural populations reciprocally coupled by inhibitory synapses that autonomously oscillate in alternation [19], [20]. The second, closed-loop control action is provided by a sensory-driven feedback, which provides information about the mechanical interaction of the animal body with the environment and secures adaptation to unexpected obstacles and uncertainties during ambulatory excursions. The third, also closed-loop control action is ensured by supra-spinal networks, which, based on sensory information (usually, mainly visual and tactile), timely inform the CPG about the rhythm (and corresponding gait) to be imposed, thus changing muscle activity. Here we consider only the first and part of the third control actions.

The reciprocal interactions of these basic mechanisms concur to the inter-limb coordination and produce flexible and efficient locomotion. The detailed biophysical mechanisms underlying locomotion are yet to be fully understood. Therefore, the current research focusing on the phenomenologically reduced CPG design (oriented towards robotic applications) pursues several development lines based on decentralized control [21], bottom-up approach with use of functional blocks [18], nonlinear dynamics and bifurcation theory [16], [22].

C. Effective variables and parameters

The existence and stability of rhythmic patterns generated by CPGs are analyzed using the so-called phase lags introduced for oscillatory or bursting cells [7], [24], [25]. All isolated/coupled cells are assumed to have and maintain relatively close temporal characteristics. In the dynamical systems terminology, this means that each i-th cell resides on a structurally stable periodic orbit of period T_i in the state space of the corresponding model. Its current position on the periodic orbit can be determined using a new phase variable $\phi_i(t) \in [0, 1)$, defined modulo 1, such that ϕ_i is reset to 0 when the voltage V_i increases above some synaptic threshold V_{th} at times $t_i^{(k)}$. The phase-lag representation of an N-cell network employs $N-1$ state variables describing the phase lags $\Delta_{1i}(t) = \phi_i(t) - \phi_1(t)$ between the spike/burst initiations in the reference cell 1 and the other ones coupled within the network. The time evolutions of these state variables, being quite complex due to nonlinear interactions, can be determined through numerical simulations. For that purpose, we compute the phase lags between coupled cells in a discrete set of time instants as:

$$\Delta_{1i}^{(k)} = \frac{t_i^{(k)} - t_1^{(k)}}{t_1^{(k)} - t_1^{(k-1)}}, \quad \text{mod } 1. \tag{1}$$

As time progresses, the phase lags $\Delta_{1i}^{(k)}$ can converge to a single or several steady or phase-locked states. The presence of multi-stability can be evidenced by integrating the system of equations governing the network densely sweeping initial conditions for phases.

The locomotion in quadrupeds is produced by the coordination of limbs movements with specific speed (frequency) and ratio between the stance and swing phase (duty cycle) and with the given phases in the repetitive patterns that drive the limbs. The coordination, i.e., the specific phase lags between the limbs, determines the animal gait, which usually changes with the speed. This modeling paper is focused on the locomotion of mice, which can exhibit four different gaits: walk (W), trot (T), gallop (G) and bound (B), with frequency f and duty cycle dc ranging in the intervals $[2, 12]$ Hz and $[0.25, 0.6]$, respectively [27], [28]. Table I summarizes the characteristics of mouse gaits, extracted from [27], [28]. Assuming that the CPG contains one cell per leg with L=left, R=right, F=fore, H=hind, we take as reference leg LF and compute the phase lags LF-RF (Δ_{12}), LF-LH (Δ_{14}), and LF-RH (Δ_{13}).

At low speed ($f < 4$ Hz), mice walk: in this gait the swing phase is shorter than the stance phase and the limbs swing one at a time. Trot occurs at medium speed ($4 < f < 9$Hz): in this gait the stance and swing phases have the same duration, left-right and fore-hind limbs move in alternation. Gallop is exhibited at medium-high speeds ($9 < f < 10$ Hz): in this gait the swing phase is slightly longer than the stance phase, left and right limbs move almost together, whereas fore and hind limbs move in alternation. At high speed ($f > 10$ Hz) mice bound: in this gait the swing phase is again slightly longer than the stance phase, fore and hind limbs move in alternation, whereas left and right limbs move together.

TABLE I
GAITS CHARACTERISTICS: FREQUENCY (f), DUTY-CYCLE (dc), PHASE-LAGS BETWEEN LEGS AND CORRESPONDING α-VALUES.

Gait	$f[Hz]$	dc	LF-RF (Δ_{12})	LF-LH (Δ_{14})	LF-RH (Δ_{13})	α
W	$[2, 4]$	< 0.4	0.5	0.25	0.75	$[0, 0.25]$
T	$[4, 9]$	$[0.4, 0.51]$	0.5	0.5	0	$[0.25, 0.5]$
G	$[9, 10]$	> 0.51	0.1	0.6	0.5	$[0.5, 0.75]$
B	$[10, 12]$	> 0.51	0	0.5	0.5	$[0.75, 1]$

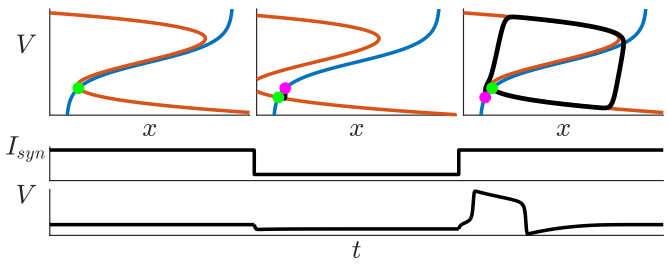

Fig. 1. Post-inhibitory rebound mechanism in B-model with the parameters listed in Appendix A, except $g_D = 0$. Top panels: Post-inhibitory trajectory (black line) in the phase space superimposed with the the fast V- and slow x-nullclines (orange and blue, resp.) crossing at the equilibrium state (green dot). Application of negative pulse (middle panel) causes first hyper-polarization followed by the post-inhibitory rebound in the cell voltage (bottom panel).

Sequential switching from one gait to another is controlled by the bifurcation parameter $\alpha \in [0, 1]$, which represents the control action provided by supra-spinal networks: the mouse speed increases with increasing α values. The transitions between these gaits occur sequentially as the parameter is increased/descreased; we chose to assign one quarter of the parameter range to each gait.

III. The Proposed Method

In this section, we propose a sequence of operating principles and steps to design a reduced CPG circuit producing a desired set of gaits.

A. Choice of the cell model: the PIR mechanism

In the design of a synthetic CPG a proper understanding of its biological functions helps one to optimize the trade-off between the unavoidable complexity of biological phenomena and the necessary simplicity of mathematical modeling. So, the models employed in this study have to possess the mechanism reproducing the so-called post-inhibitory rebound (PIR) of the cell membrane voltage, which occurs as soon as the post-synaptic quiescent cell is abruptly released from hyper-polarizing inhibition (e.g., due to an external current pulse) or from another pre-synaptic cell of the network. The PIR mechanism allows two reciprocally inhibiting cells to generate self-sustained oscillations [19], [29]. In particular, in a half-center oscillator made of two cells coupled reciprocally with fast inhibitory synapses, this mechanism lets the half-center oscillator generate self-sustained spiking/bursting in alternation. This effect is qualitatively illustrated in Fig. 1 for an isolated cell described by model B in Appendix A. The model has two dynamic variables, V, and x, representing the fast voltage and slow gating variables, respectively. The top panel of Fig. 1 shows the (x, V)-phase portrait with the fast Z-shaped nullcline (orange line) on which $\dot{V} = 0$ and the slow nullcline (blue line) on which $\dot{x} = 0$. Their only intersection point to the right of the knee on the low branch of the V-nullcline is a stable equilibrium state (marked as the green dot) of the model, corresponding to the quiescent hyper-polarizing state of the cell. Due to the slow-fast nature of the model, its solutions converge to this state following the shape of the fast nullcline. The negative pulse of external current I_{syn}, leaving the x-nullcline intact, makes the V-nullcline shift to the left so that the stable equilibrium state of the unperturbed system (marked by the purple dot in the top-central panel) moves below and to the left (green dot) in the V-nullcline of the perturbed system. Correspondingly, $V(t)$ drops down (bottom panel). We note that the PIR-mechanism requires three necessary conditions be met: the hyper-polarizing perturbation, due to either an external pulse or the inhibitory current, must be (1) strong and (2) long enough and (3) must have a rapid termination phase. This means that the ascending front of the pulse must be nearly vertical as one shown in the middle panel in Fig. 1, and the synapse must be fast, not slow. After I_{syn} is abruptly turned off, the state (x, V) starts from the position of the disappeared equilibrium point (purple dot in the top-right panel), follows the upper and lower branches of the V-nullcline and converges back to the original equilibrium point (green dot), tracing down a transient excursion (black thick trajectory in the top-right panel) corresponding to the outburst in the voltage trace (bottom panel).

In our CPG model, a cell is described by the following state equation:

$$\dot{\mathbf{z}}_i = \begin{bmatrix} \dot{V}_i \\ \dot{\mathbf{x}}_i \end{bmatrix} = \begin{bmatrix} f_i(\mathbf{z}, I_{syn}^{(i)}(\alpha), g_D D_i(\alpha)(V_i - E)) \\ \mathbf{p}_i(\mathbf{z}_i) \end{bmatrix}, \quad (2)$$

where V_i is treated as the membrane potential of the i-th cell, while $\mathbf{x}_i$ represents its gating variables and $I_{syn}^{(i)}$ is its incoming synaptic current. The term $g_D D_i(\alpha)(V_i - E_{ex})$ describes an overall influence (modulated through the α-parameter) of the supraspinal networks on the given postsynaptic cell.

To examine and tune up the CPG outcomes, in this paper we adopt three models of its cells that all exhibit the PIR. These are the conductance-based model used in [30] (code-named model A), a generalized FitzHugh-Nagumo model [8] (model B), and the adaptive exponential integrate-and-fire model [31] (model C) that can generate also bursting activity. They are described in Appendix A.

B. Choice of the synapse model

The synapses in our CPG models are required to demonstrate a rapid time course [20]. Here, we consider three models of such fast synapses: the first two ones are represented by the fast threshold modulation (FTM) synapses [32], with different activation functions, namely given by the sigmoidal (model β) and step-wise (model γ) functions; the third model is the dynamical α-synapse (model δ) [19], [33], which in general is not necessarily fast.

In a CPG composed of N cells, we introduce the action of inhibitory, excitatory and delayed inhibitory chemical synapses on the i-th cell as follows

$$\begin{aligned} I_{syn}^{(i)}(\alpha) = \sum_{j=1}^{N} \{ & g_{ij}^{in} A(V_j(t), s_{in}(t))(E_{in} - V_i(t)) + \\ & g_{ij}^{di} A(V_j(t - \tau), s_{di}(t))(E_{in} - V_i(t)) + \\ & g_{ij}^{ex}(\alpha) A(V_j(t), s_{ex}(t))(E_{ex} - V_i(t))\}, \end{aligned} \quad (3)$$

where $I_{syn}^{(i)}$ is the current injected into the i-th cell, V_i and V_j are the membrane potentials in the post- and pre-synaptic

cells, s_{xx} is the synapse state (only for dynamical synapses), g_{ij}^{xx} is the maximal synapse strength, $A(V_j, s_{xx})$ is the synapse activation function (A depends on the state only for dynamical synapses), E_{xx} is the synapse reverse potential, and τ is the synapse delay; here in, di and ex stand for inhibitory, delayed inhibitory and excitatory, respectively.

We notice that, as described in Sec. III-C, the weights of the excitatory synapses vary with changes in α values to reproduce the effect of the brainstem on the excitatory interneuron populations in a real CPG.

C. Network assembly-line: operating principles

Our network governing the mice locomotion results from a reduction of the 40-cell CPG proposed in [30] to regulate both speed and gaits of the mouse. The 40-cell CPG is made of four blocks of rhythm-generators (RG), each driving a limb, that are all cross-linked through inhibitory and excitatory interneuron populations. Each RG contains two populations, flexor and extensor, which inhibit each other and control the swing and stance phases of the limbs. In particular, when the flexor (extensor) population is active, the corresponding limb is in the swing (stance) phase. The gait generated by the CPG can be controlled through variations of α.

To simplify the 40-cell CPG, we employ the strategies proposed in [14], [16], which can be summarized in three steps: (A) substitute the interneuron populations with fast chemical synapses, inhibitory or excitatory, depending on the nature of the replaced population; (B) remove the extensor populations; swing phase is still regulated by the flexor units, whereas the stance phase is activated when the flexor units are silent; (C) add inhibitory delayed synapses between left and right cells to reproduce the action of extensor populations.

We remark that step A can be achieved using several inhibitory pathways, as shown in Fig. 2. In particular, the simplified two-cell circuit shown in Fig. 2c can model both the inhibitory pathways shown in Figs. 2a and 2b, which are commonly found in biological neural circuits [34], [35]. The resulting simplified CPG circuit is shown in Fig. 3a. It contains four numbered cells only, each one driving a particular limb, labeled as follows: L=left, R = right, H = hind, F = fore. They are cross-connected with fast inhibitory (gray), excitatory (black) and delayed inhibitory (orange) synapses. An equivalent yet compact notation for the circuit is presented in Fig. 3b. The circuit in Fig. 3 has a general structure that might represent not only a simplified biologically-inspired CPG, but also some generic synthetic CPG (with only homolateral and

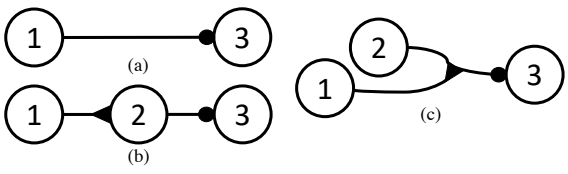

Fig. 2. Reduced circuit (a) representing two typical inhibitory 3-cell pathways where either cell 1 first excites the middle cell 2 that next inhibits cell 3 (b), or excitatory cell 1 facilitates the inhibition projected from cell 2 onto the postsynaptic cell 3 (c). Inhibitory and excitatory synapses are marked by circle •- and triangle △-shaped terminals, respectively.

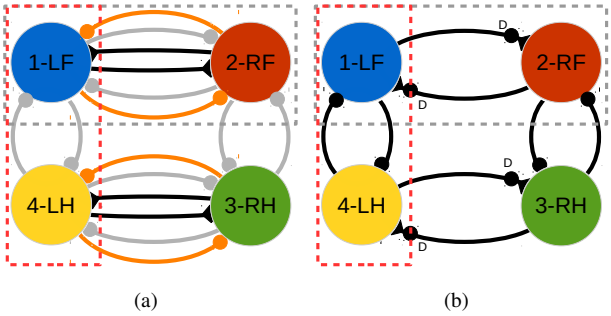

Fig. 3. Proposed 4-cell CPG to govern the mouse locomotion, with the complete (a) and compact (b) circuitry. The four numbered cells are cross-connected with synapses: fast inhibitory (marked by grey/black dots • in (a)/(b)), delayed inhibitoty (orange dots in (a) and marked with *D* in (b)), and excitatory (black triangles △).

commissural connections) with four cells to regulate limb flexors in quadrupeds. Similar spatio-symmetric circuits have been identified in various biological CPGs, including swim CPGs in the mollusks *Melibe leonina* and *Dendronotus iris* [36]–[38]. In other words, the CPG topology can be either bio-inspired or assigned/decided by the designer.

D. Parameter selection strategy

We describe our parameter selection strategy by employing the same cell and synapse models as in [14]. This allows us to both illustrate our design method and validate the obtained results by comparison with this benchmark.

Once the CPG topology is defined (either by simplifying a bio-inspired model or by making direct reference to a structure relying on symmetry properties), we first have to choose which CPG parts depend on the α parameter. In the case of bio-inspired architectures, this information can be simply inferred from the original CPG. For synthetic CPGs, we can follow two guidelines: (i) all cells have to depend on α, in order to make frequency and duty cycle α-dependent; (ii) about synapses, we assume as α-dependent those that allow us to break symmetries, thus enabling gait transitions. Of course, more refined strategies could be used: for instance, one can decide that *a priori* all synapses depend on α and then check *a posteriori* which connections show an effective dependence on the brainstem control. The price to be paid would be an increase in the computational costs. This is an open problem, and the solution proposed here is a trade-off between computational complexity in the design phase and accuracy of the obtained model.

Summing up, in our case-study we assume that all cells (through the function $D_i(\alpha)$) and all excitatory synapses (through the strengths $g_{ij}^{ex}(\alpha)$) depend on α, as pointed out in Eqs. (2) and (3), whereas we fix the inhibitory synapses strengths g_{ij}^{in} and g_{ij}^{di} to the values listed in Appendix B.

For the sake of simplicity, we assume that the functions $D_i(\alpha)$ and $g_{ij}^{ex}(\alpha)$ are piecewise-linear (PWL). We calibrate these functions in order to make our CPG able to produce all gaits listed in Table I. To this end, we make the following steps, with the aid of the computational toolbox CEPAGE [15].

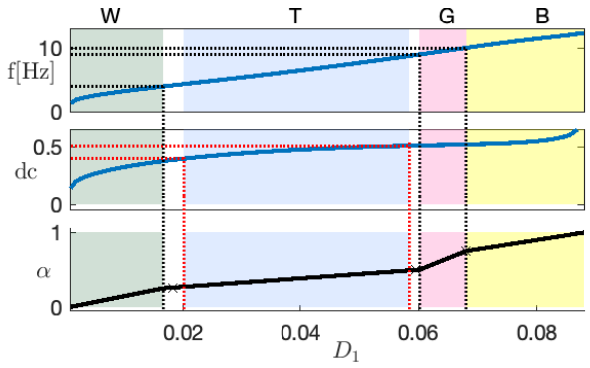

Fig. 4. Frequency f (top panel) and duty cycle dc (middle panel) plotted against the driving function $D_1(\alpha)$ of the control parameter α (bottom panel). Dotted lines demarcate the boundaries for each gait (see Tab. I). Crosses indicated the landmarks used to define the function $D_1(\alpha)$. White regions correspond to co-existing stable gaits.

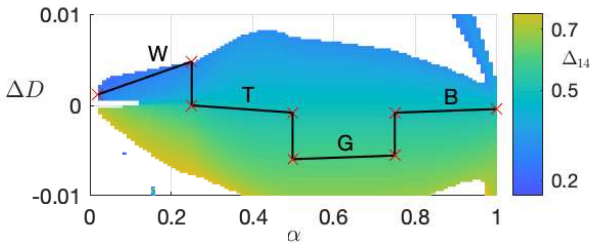

Fig. 5. Bifurcation diagram in the $(\alpha, \Delta D)$-parameter plane. It is color-mapped according to the values of the phase-locked lag Δ_{14} (vertical bar on the right). The CPG is silent in the white regions and generates rhythmic outcomes in the color regions. Red crosses label the landmarks used to define the function $\Delta D(\alpha)$ (PWL black line).

Step 1. Clock tuning (acting on the fore cells): Let us focus on the reference cell 1 isolated from the rest of the CPG. We first assess spike frequency f and duty cycle dc of the state variable $V_1(t)$ for a range of D_1-values. For instance, the bifurcation diagram shown in Fig. 4 is built on a 1D 100-long array of equidistant D_1-values. We remark that D_1 influences the behavior of cell 1, according to Eqs. (2) and (4). The D_1 range is chosen so that the cell is not quiescent. The figure illustrates how the frequency f (top panel) and the duty cycle dc (middle panel) of the generated membrane voltage $V_1(t)$ vary as D_1 is increased. These plots (numerically obtained using the CEPAGE package) are used to identify the D_1 ranges corresponding to the different gaits according to Tab. I. For instance, the green region corresponds to walk, as in the D_1 range $[0, 0.017]$ the frequency range is $[2, 4]$Hz and dc remains below 0.4. The same holds for the other colored regions.

Next, we choose the monotonically increasing PWL function $D_1(\alpha)$ passing through a set of selected landmarks. The PWL function $D_1(\alpha)$ is chosen so that, while α increases from 0 to 1, both f and dc increase monotonically between their minimum and maximum values given in Tab. I: f ranges between 2Hz and 12Hz, whereas dc varies between 0.25 and 0.65. To this end, we set some landmarks on the plane (D_1, α) (bottom panel): we chose to set them at the transitions between the gaits, imposing that these transitions happen at the values $\alpha = 0.25, 0.5, 0.75$, according to Tab. I. The PWL function $\alpha(D_1)$ (black thick curve) is a mere linear interpolation of these landmarks and its inverse is the desired function $D_1(\alpha)$. Finally, we set $D_2(\alpha) = D_1(\alpha)$, as cell 2 (when isolated) is identical to cell 1. Through this step, we exploit brute-force bifurcation analysis to establish a direct dependence of f and dc for the fore cells on α, by properly defining the PWL function $D_1(\alpha)$, which influences the cell dynamics, according to Eq. (2).

Step 2. Fore-hind coordination (acting on the hind cells): Now we consider the neural circuit within the dashed red rectangle in Fig. 3 and set $D_4(\alpha) = D_1(\alpha) + \Delta D(\alpha)$. Next, we perform the bifurcation analysis to find the PWL function $\Delta D(\alpha)$, which ensures the desired synchronization between cells 1 and 4, i.e., between the hind and fore limbs. To this end, we obtain a brute-force 2D bifurcation diagram by plotting the asymptotic phase-lag Δ_{14} for a grid of values of ΔD and α. For instance, the bifurcation diagram in Fig. 5 corresponds to a 2D (α, ΔD)-parameter sweep on a uniform 200×200-grid of the parameter values. In the white regions the CPG does not oscillate, as cells 1 and/or 4 remain inactive. In the colored region, Δ_{14} varies in the range $[0.25, 0.7]$. This means that the left-hand-side half-center oscillator made of cells 1 and 4 (which is in charge of the front-hind synchronization) can exhibit a great capacity of asymptotic phase-locked states, which, in turn, ensures a large variability in the gaits. Next, we define the function $\Delta D(\alpha)$ so that it passes through a set of selected points, on the (α, ΔD)-sweep diagram. To select the landmarks (indicated by red crosses in Fig. 5), we focus again on the transitions between different gaits. For instance, the walk gait corresponds to $\Delta_{14} = 0.25$ (see Tab. I). Therefore, we place two landmarks with α coordinates 0 and 0.25 (bounds of the walk gait, see Tab. I) and ΔD coordinates corresponding to dark blue pixels, i.e., to the phase-locked lag LF-LH $\Delta_{14} = 0.25$. Moreover, in order to ensure that the gait is maintained within the whole α-interval, we choose the two landmarks such that the connecting segment lies over dark blue pixels. By following the same line of reasoning for all gaits, we define $\Delta D(\alpha)$ as the PWL function connecting the landmarks, as shown (black line) in Fig. 5: the PWL curve stays within the color regions in the parameter space and each segment of $\Delta D(\alpha)$ corresponds to a specific gait (corresponding to a color) occurring within the given α-window. Finally, we set $D_3(\alpha) = D_4(\alpha)$ in virtue of the network symmetry.

Step 3. Left-right coordination (acting on the synapses): In this step we tune up the neural circuit singled out within the dashed gray rectangle in Fig. 3 and set $g_{21}^{ex}(\alpha) = g_{12}^{ex}(\alpha) = g^{ex}(\alpha)$ (strength of the black synapses), as there is experimental evidence [3] that the brainstem control acts in the same way on the synapses connecting cells 1-2 and 3-4. As for the previous steps, the PWL function $g^{ex}(\alpha)$ is defined by exploiting bifurcation analysis, in order to ensure the desired synchronization between left and right cells. First, we find the phase-locked lag Δ_{12} for an array of values of g^{ex} and α to get another brute-force 2D bifurcation diagram. Figure 6 shows the results of a 2D (α, g^{ex})-parameter sweep on a uniform 200×200-grid for our case-study. In the upper part of the bifurcation diagram (dark blue region) the cells

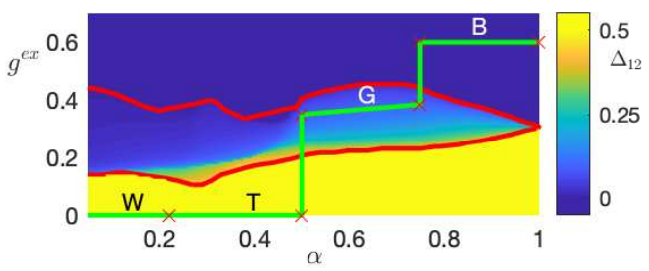

Fig. 6. Bifurcation diagram in the (α, g^{ex})-parameter plane, color-mapped according to the values of the phase-locked lag Δ_{12} (vertical bar on the right). Landmarks (red crosses) are used to define the PWL function $g^{ex}(\alpha)$ (green curve).

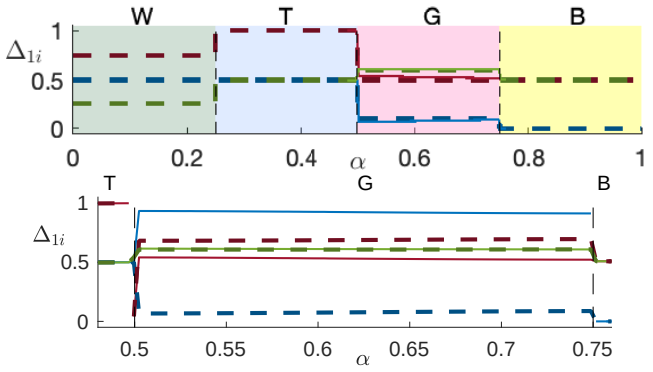

Fig. 7. Top panel: desired (dashed lines) and simulated (solid lines) phase-locked lags Δ_{1i}, with $i = 2$ (blue lines), $i = 3$ (red lines) and $i = 4$ (green lines), plotted versus α. The colors evidence the existence windows corresponding to the four gaits: walk, trot, gallop and bound. Bottom panel: enlargement with $\alpha \in [0.475, 0.775]$ demonstrating bistability for the gallop gait due to the forward and backward pitchfork bifurcations that give rise to two possible asymptotic phase-lag Δ_{1i} (shown as dashed and solid lines), for $i = 2$ (blue) and $i = 4$ (red). For $i = 3$ (green) there is only one steady-state phase-lag.

synchronize in-phase ($\Delta_{12} = 0$), whereas in the lower part (yellow region) they synchronize in anti-phase ($\Delta_{12} = 0.5$), according to the color-bar for the phase-lag Δ_{12} on the right-hand side. In the central region, marked with two red curves, the network becomes bi-stable and can generate two distinct rhythmic patterns. This bi-stability is due to two pitchfork bifurcations, forward and backward, occurring at the parameter values marked by the red lines, found with a brute-force numerical analysis through CEPAGE. In this bistability region, there are two stable equilibrium states: one associated with the phase-coordinate $0 \leq \Delta_{12} \leq 0.5$, and its mirror-image with phase $(1 - \Delta_{12})$.

Finally, we define the function $g^{ex}(\alpha)$ so that it passes through a set of landmarks in the found bifurcation diagram. Just to set the ideas (the gait order is unessential, in this step), we start calibrating the CPG circuit so that it can produce the bound gait, with the desired phase-locked lags LF-RF (see Tab. I). This gait requires $\Delta_{12} = 0$, and therefore the range of the driving function $g^{ex}(\alpha)$ must lie within the dark blue region in Fig. 6. For simplicity, we pick $g^{ex}(\alpha) \simeq 0.6$ for $0.8 \leq \alpha \leq 1$. Next, we select $g^{ex}(\alpha) = 0$, for $0 \leq \alpha \leq 0.5$, corresponding to the walk and trot gaits, characterized by $\Delta_{12} = 0.5$. Finally, for the gallop at the mid speed, we select a set of landmarks (red crosses) yielding $\Delta_{12} \simeq 0.1$ in the central region of the bifurcation diagram. On the whole, the function $g^{ex}(\alpha)$ is the PWL green curve shown in Fig. 6.

Using the same strategy, we can independently calibrate the subnetwork controlling the phase lag LH-RH Δ_{34} by selecting the corresponding PWL functions $g^{ex}_{34}(\alpha) = g^{ex}_{43}(\alpha)$. The results are completely similar (even if not equal, as $D_1(\alpha) \neq D_3(\alpha)$) to those found in Fig. 6 and hence are not discussed here for the sake of conciseness.

Step 4. Complete CPG (*a posteriori* validation): Since the previous steps, acting locally, do not fully guarantee that the complete CPG dynamics is as desired, in the last step we need to verify the overall CPG behavior. To do that, we simulate the CPG performance by employing the PWL function selected in the previous steps for a grid of values of α and we compare the obtained asymptotic phase lags with the values in Tab. I.

The top panel in Fig. 7 shows the desired (dashed lines) phase-locked lags Δ_{1i} from Tab. I plotted against the control parameter α for our case-study: Δ_{12} (blue lines), Δ_{13} (red lines) and Δ_{14} (green lines), between the cells of the CPG. They overlap almost everywhere with the simulated ones (solid lines) for all four gaits: walk, trot, gallop, and bound. One can easily verify that the phase lags meet the requirements (legs' movements) described in Sect. II-C: for instance, in the walk gait the four cells activate sequentially in the order 1–4–2–3, as shown in the top panel of Fig. 8.

As we pointed out above, at the transitions from trot to gallop

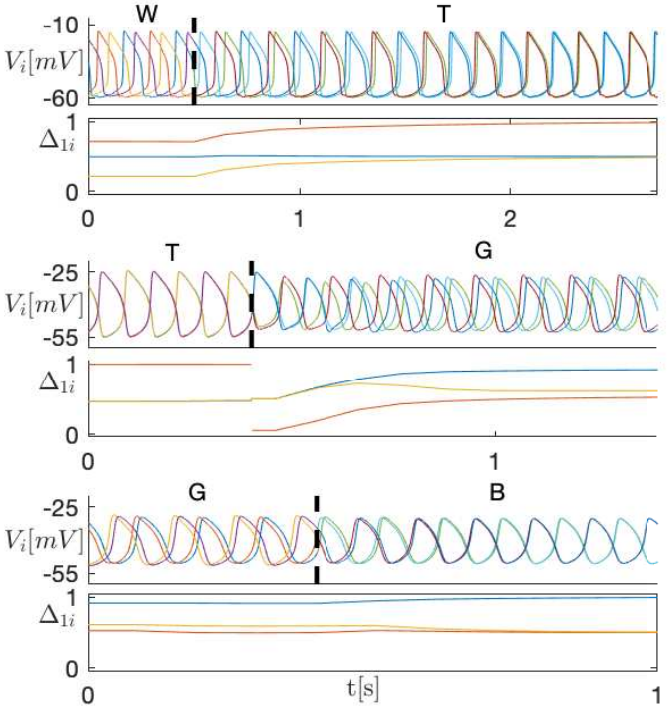

Fig. 8. Time-plots of the "membrane potentials" V_i, and phase-lags Δ_i, at gait transitions: from walk to trot (top), from trot to gallop (middle), and from gallop to bound (bottom). The colors of the $V_i(t)$ curves are matched with those of the corresponding cells in Fig. 3.

and from gallop to trot, two pitchfork bifurcations occur. This causes the effect of bistability in the gallop region, as magnified in the bottom panel of Fig. 7. Both stable equilibrium states in the 3D $(\Delta_{12}, \Delta_{13}, \Delta_{14})$-phase space of the network system correspond to the same gallop gait, though with reverse order of moving limbs.

To check that the CPG switches smoothly between gaits, Fig. 8 shows the time evolution of the membrane voltages V_i and of the phase-lags Δ_{1i} of the network when α is increased smoothly across the edge between: walk and trot (top), trot and gallop (middle), gallop and bound (bottom) regions. It is apparent (from both the time and phase-lag plots) that all gait transitions are smooth.

In summary, the original CPG circuit can be effectively reduced at the cost of a reasonable complication of the synaptic connectivity. The desired gaits are achieved by affecting the reference cell and its synaptic connections with other cells of the network. The synaptic strengths and each cell model depend on the single control parameter α. The specific profiles of these dependences are chosen through a design strategy based on the methods of nonlinear dynamics and bifurcation analysis. The network symmetry allows us to use many simplifications to calibrate the CPG step-by-step, first at the cellular and further at the network level. We set the reference cell (here 1) to define the dependence of the spike frequency f and duty cycle dc on the single control parameter α. Then, we find the conditions to maintain the proper phase-locked lags among all four cells for the given gait.

We remark that this design strategy cannot ensure *a priori* to obtain all the desired gaits, as pointed out in the next section: therefore, the behavior of the resulting CPG must be always checked *a posteriori* (step 4). Moreover, many parts of the method can be changed, as there exist multiple ways to realize this process. For instance, the choice of the interpolation strategy or of the reference cell.

Finally, we remark that this strategy is suitable for networks with a limited number of cells. By construction, the principal limitation of our method is that we have to verify that the CPG under design keeps the features learned during the previous steps. For CPGs with large cell numbers, it would become increasingly difficult to obtain through our local strategy functions of α that well capture the behavior of the network. On the other hand, the prime focus of our approach is designing simple CPGs with the basic functional mechanisms underlying locomotion. Therefore, from this standpoint, the fact that our method works well for simple CPGs is hardly a limitation but a gain.

IV. Robustness of the design strategy

This section is a showcase of the results obtained for four further CPGs, with the same wiring diagram in Fig. 3, that are made of different cell and synapse models, see Appendices A and B. While preserving the network topology, we test different synapse and cell models to verify the robustness of the proposed design strategy.

Each CPG is symbolically labeled as $[x/y]$ with the employed cell/synapse models (see Appendices A and B). In the first two CPGs with the tandems: $[B/\beta]$ and $[C/\beta]$, we consider two alternative cell models, whereas in the other two CPGs, namely $[A/\gamma]$ and $[A/\delta]$, we examine how two alternative synaptic models can alter the network dynamics. We remark that the parameters of the dynamical synapse model δ are chosen in order to ensure fast dynamics, according to Sec. III-B. To build these CPGs we follow the checklist described in Sec. III-D.

As pointed out in Sec. III-D, our method to set the landmarks and obtain the required PWL functions does not need a high resolution of the bifurcation diagram. It is sufficient to get a rough idea of the color regions. This is of course an advantage, from a computational standpoint, and for this reason the bifurcation diagrams in this section are quite rough.

Step 1. The starting point is the calibration of the cell model. Fig. 9 shows a 1D bifurcation sweep (on an array of 100 uniformly spaced D_1 samples) of the spike frequency f and duty cycle dc that are plotted against D_1 in models B and C. As far as model C is concerned (Fig. 9b), variations of D_1 properly influence both the frequency (top panels) and the duty cycle (middle panels) of every cell of the network. However, in model B (Fig. 9a), the ranges of the frequency and duty cycle do not cover all the values necessary for the CPG-network to produce all four gaits (see Tab. I). So, $[B/\beta]$-CPG can only produce walk (left light green region) and trot (central light-blue region in Fig. 9a). For this reason, we select the PWL function $D_1(\alpha)$ only for $\alpha \in [0,\, 0.5]$. On the contrary, model C can well generate all the required f and dc values when we choose the PWL function $D_1(\alpha)$ as described in Sec. III-D. The obtained results are coherent with the model complexity and biological plausibility levels. We remark that the parameters of model C are set in order to have bursting activity, instead of spiking as in the other cases.

Step 2. Bifurcation diagram in Fig. 10 is the $(\alpha, \Delta D)$-parameter sweep of Δ_{14} on a grid of 100×100 parameter values. The white spaces correspond to the regions where cells 1 and/or 3 become quiescent. Therefore, we focus on the colored regions. All the proposed CPGs are able to generate for each value of α an asymptotic phase lag Δ_{14} in the range $[0.25, 0.65]$, so cells 1 and 4 can regulate front and hind limbs to move with a plethora of phase lags, thus producing different gaits. To select the landmarks and the PWL functions in Fig. 10 we employ the strategy described in Sec. III-D. We remark once more that for CPG$[B/\beta]$ (see Fig. 10a) we compute the diagram only for $\alpha \in [0, 0.5]$ because this CPG can only produce walk and trot gaits.

Step 3. The bifurcation diagram depicted in Fig. 11 is the bi-parametric sweep on a grid of 50×50 (α, g^{ex}) pairs. One can observe a similarity in all panels, particularly, in the upper part (dark blue region) where the cells synchronize in phase with $\Delta_{12} = 0$, whereas in the lower part (yellow region) they synchronize in anti-phase with $\Delta_{12} = 0.5$. The red lines mark pitchfork bifurcations bounding bistability regions in the diagram. Overall, we can obtain any phase lag, Δ_{12} ranging from 0 to 1. All CPG circuits, except for the $[A/\gamma]$ tandem, can generate the necessary phase-lags Δ_{12}. Specifically, the $[A/\gamma]$-CPG does not yield $\Delta_{12} = 0.5$ (as a unique solution) when $\alpha \in [0.3, 0.4]$, and therefore it does not produce the trot

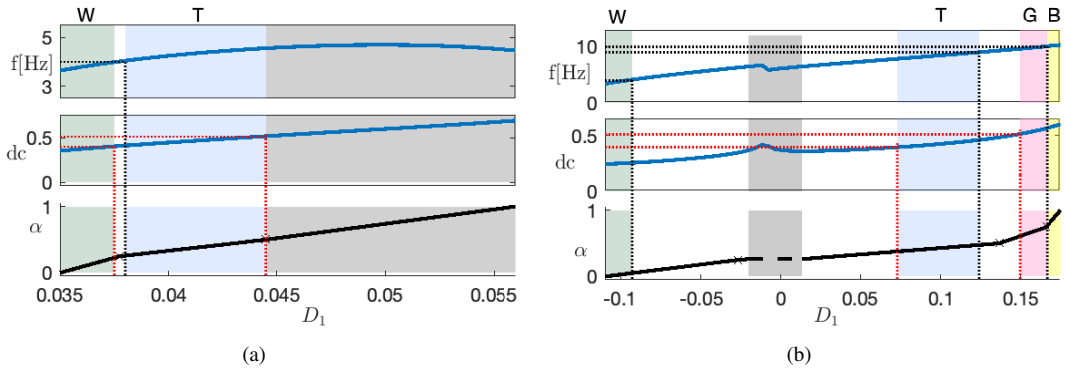

Fig. 9. Step 1. Frequency f (top panels), duty cycle dc (middle panels) plotted against D_1 for cell models B (a) and C (b). Dotted lines demarcate the boundaries for each gait (see Tab. I). Crosses indicate the landmarks to define and calibrate the functions $D_1(\alpha)$, whose inverse functions $\alpha(D_1)$ are shown in the bottom panels. Gray regions do not correspond to any mouse gait, while white regions of f and dc correspond to multiple stable gaits.

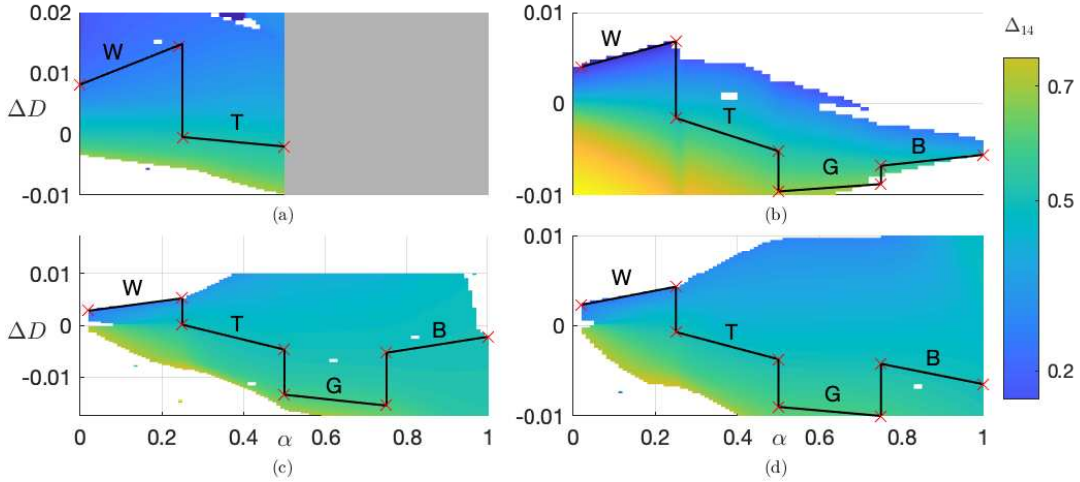

Fig. 10. Step 2. Bifurcation diagrams in the $(\alpha, \Delta D)$-parameter plane for cell-synapse models: $[B/\beta]$ (a), $[C/\beta]$ (b), $[A/\gamma]$ (c), and $[A/\delta]$ (d). White spaces are composed of parameter pairs corresponding to quiescent cells. Red crosses represent the landmarks to define and calibrate the function $\Delta D(\alpha)$ (PWL black graph). Gray region in panel (a) denotes a not feasible interval of α-values.

gait. This limitation is due to the synapse γ-model, which is not continuous. On the contrary, the more realistic δ-model provides the results shown in Fig. 11d, that are coherent with those shown in Fig. 6. We re-iterate that the methodology to define the PWL functions $g^{ex}(\alpha)$ (green lines in Fig. 11) is the same as in Sec. III-D.

Step 4. The four panels in Fig. 12 show the desired (dashed lines) phase-locked lags Δ_{1i} overlaid with the simulated ones (solid lines) for the four CPG models. The $[C/\beta]$- and $[A/\delta]$-CPGs can generate all four gaits within the whole range of α values. As expected, $[B/\beta]$-CPG generates only walk and trot gaits because, as described in Step 1, it is out of reach of the frequency and the duty cycle associated with gallop and bound. $[A/\gamma]$-CPG, as described in Step 3, does not generate trot as a unique gait within $\alpha \in [0.3, 0.4]$ (gray region on the left in Fig. 12a). Moreover, this CPG cannot generate gallop, probably due to the excessive roughness of the synapse model.

The results obtained on the complete CPGs are indicative that their dynamics are not strongly dependent on the synapse or/and cell models employed, provided that they are not too oversimplified.

V. Conclusions

We proposed a 4-step method for the design of synthetic CPGs able to produce a prescribed set of gaits. Our strategy requires that both cells and synapses meet some generic assumptions: each cell has to possess the PIR mechanism and each synapse must be fast, even if it is delayed. In the absence of the PIR mechanism, Δ_{14} would span smaller ranges, thus making the dynamics of the CPG less controllable. In turn, this makes it more difficult to stably realize all the prescribed gaits. Moreover, obtaining the small phase lags needed to produce some gaits is more problematic with slow synapses [20]. The "richness" of the cell models plays another key role: more accurate and adequate models allow one to accomplish the design priorities more easily. For instance, with model B (simpler than model A), the occurrence of two out of the four prescribed gaits happened to be unmanageable.

Our method can be applied either to reduce a biological CPG or to an assigned CPG topology. Generally speaking, with our method one can reduce any biological CPG to its synthetic surrogate with similar rhythm generation. Alternative reduction strategies can be further developed by resorting to cluster synchronization methods [39], for instance, provided

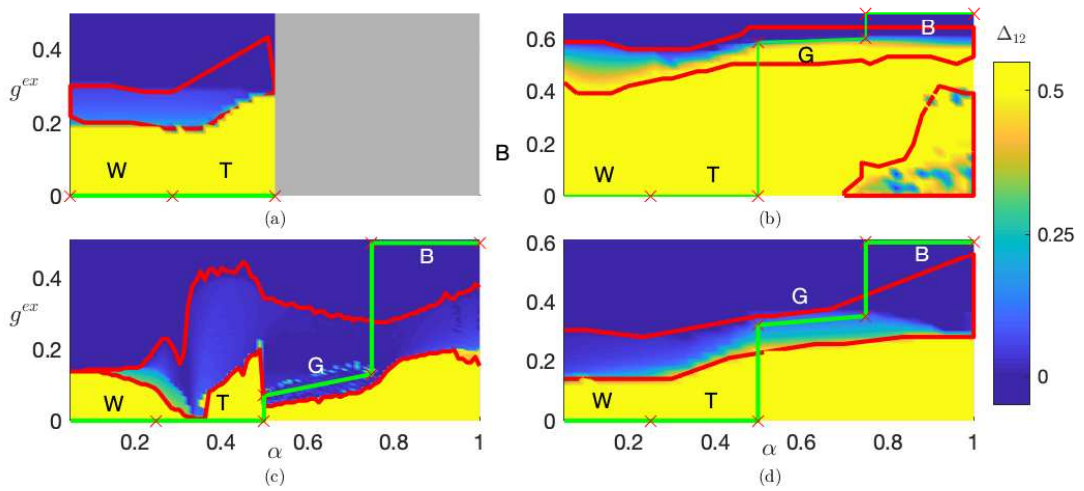

Fig. 11. Step 3. Bifurcation diagrams in the (α, g^{ex})-parameter plane for cell-synapse CPG tandems: $[B/\beta]$ (a), $[C/\beta]$ (b), $[A/\gamma]$ (c), and $[A/\delta]$ (d). Red crosses indicate the landmarks to define the function $g^{ex}(\alpha)$ (PWL green graph). Red lines mark the pitchfork bifurcations bounding the bistability regions.

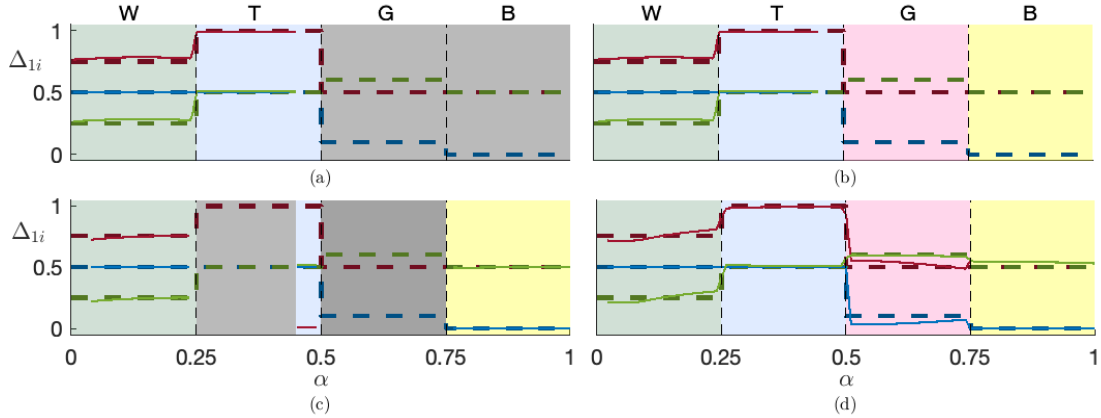

Fig. 12. Step 4. The desired (dashed lines) and simulated (solid lines) phase-locked lags Δ_{1i}, $i = 2$ (blue), $i = 3$ (red) and $i = 4$ (green) for cell-synapse model tandems: $[B/\beta]$ (a), $[C/\beta]$ (b), $[A/\gamma]$ (c), and $[A/\delta]$ (d). The bifurcation diagram is subdivided into four regions corresponding to the desired gaits: walk, trot, gallop and bound. Gray regions are α-intervals without stable gaits.

that they are applicable for heterogeneous networks. Other methods, particularly, those based on the mathematical theory of *groupoids*, aim to find the minimum-size network architecture producing formal phase-locking patterns [40], regardless of stability and particularities of cell and synapse models. For instance, the minimum-size CPG model for quadrupeds requires eight cells and overall six underlying assumptions [41]. Note that gait transitions, often depending on the specifics of cell and synapse types, are typically ignored or neglected *a priori* by these methods. Other approaches for managing gait transitions are discussed in [42].

The principal limitation of our method is that it relies on local properties of the CPG at each step. While this deterministic approach works well for simple CPGs, it may become less manageable for larger networks that are expected to produce more complex multi-phase dynamics. On the other hand, one of the main aims of our approach is the development of the design principles for simple CPGs, with the focus on the basic functional mechanisms underlying locomotion.

The main applications of our reduced models (in addition to their contribution in understanding the basic mechanisms producing locomotion in living beings) are in the field of robotics [42], [43] and rehabilitation [44], [45].

Appendix A
Cell Models

A. A-model

This model, used in [30], is described by the following equations:

$$
\begin{aligned}
&C\frac{dV_i}{dt} = -I_{Na} - I_L - g_D D_i(\alpha)(V_i - E_{ex}) + I_{syn}^{(i)},\\
&\tau\frac{dh_i}{dt} = h_\infty - h_i, \quad I_L = g_L(V_i - E_L),\\
&I_{Na} = g_{Na} m h_i (V_i - E_{Na}), \quad m = \left(1 + e^{\frac{V_i - V_m}{k_m}}\right)^{-1},\\
&h_\infty = \left(1 + e^{\frac{V_i - V_h}{k_h}}\right)^{-1}, \quad \tau = \tau_0 + \frac{\tau_M - \tau_0}{\cosh(\frac{V_i - V_\tau}{k_\tau})},
\end{aligned}
\tag{4}
$$

where $C = 10$pF, $g_L = 4.5$nS, $E_L = -62.5$mV, $g_{Na} = 4.5$nS, $E_{Na} = 50$mV, $V_m = -40$mV, $k_m = -6$mV, $V_h = -45$mV,

$k_h = 4$mV, $\tau_0 = 80$ms, $\tau_M = 160$ms, $V_\tau = -35$mV, $k_\tau = 15$mV and $g_D = 10$nS.

B. B-model

This generalized FitzHugh-Nagumo model proposed in [8] is described by the following equations:

$$\begin{cases} \tau \dot{V}_i = V_i - V_i^3 - x_i + I - g_D D_i(\alpha)(V_i - E_{ex}) + I_{syn}^{(i)} \\ \dot{x}_i = \varepsilon(X_\infty - X_i), \quad X_\infty = \frac{1}{1+e^{-4V_i}}, \end{cases} \tag{5}$$

where $\tau = 6.75$ms, $I = 0$, $g_D = 10$, $E_{ex} = 1.15$, $\varepsilon = 0.15\text{ms}^{-1}$.

C. C-model

This adaptive exponential integrate-&-fire model [31] is described by the following equations:

$$\begin{aligned} C\frac{dV_i}{dt} &= -g_L(V_i - E_L) + g_e e^{\frac{V_i - V_T}{\Delta_T}} + \\ &\quad - g_D D_i(\alpha)(V_i - E_{ex}) - u_i + I + I_{syn}^{(i)}, \\ \tau_w \frac{du_i}{dt} &= a(V_i - E_L) - u_i, \end{aligned} \tag{6}$$

subject to the reset rule

$$\text{if } V_i > 20, \text{ then } \begin{cases} V_i \leftarrow V_r \\ u_i \leftarrow u_i + b, \end{cases} \tag{7}$$

where $C = 501.8$pF, $g_L = 30$nS, $E_L = -70.6$mV, $V_T = -50.4$mV, $\Delta_T = 2$mV, $E_{ex} = 20$mV, $\tau_w = 71.4$ms, $a = 4$nS, $b = 100$pA, $V_r = -45$mV, $I = 800$pA, $g_e = 25$pA and $g_D = 10$nS.

APPENDIX B
SYNAPSE MODELS

A. β-model

Model β follows the fast-threshold modulation (FTM) paradigm [32]: $A(V) = \dfrac{1}{1 + e^{-\nu_\beta(V - \theta_\beta)}}$.

B. γ-model

In this model, the activation (non state-dependent) is $A(V) = H(V - \theta_\gamma)$, where $H(\cdot)$ is the Heaviside function.

C. δ-model

This dynamical so-called α-synapse model [33], [46] has a state equation given by:

$$\dot{s} = a(1 - s)\frac{1}{1 + e^{-\nu_\delta(V - \theta_\delta)}} - b\, s, \tag{8}$$

with the activation function given by $A(V, s) = \dfrac{a + b}{a} s$.

D. Synapse parameters

The synapse strengths are listed in Tab. II, whereas the values of the other parameters are listed in Tab. III.

TABLE II
SYNAPSES STRENGTH.

Parameters	values	Parameters	values
g_{12}^{in}, g_{12}^{in}, g_{34}^{in}, g_{43}^{in}	$g_0^{in} \cdot 0.2984$	g_{14}^{in}, g_{23}^{in}	$g_0^{in} \cdot 0.1241$
g_{12}^{di}, g_{12}^{di}, g_{34}^{di}, g_{43}^{di}	$g_0^{di} \cdot 0.0221$	g_{32}^{in}, g_{41}^{in}	$g_0^{in} \cdot 0.0532$
g_{12}^{ex}, g_{12}^{ex}	$g_{12}^{ex}(\alpha)$	g_{34}^{ex}, g_{43}^{ex}	$g_{34}^{ex}(\alpha)$

TABLE III
SYNAPSES PARAMETERS FOR ALL THE EMPLOYED CELL MODELS.

Synapse	Parameters	model A	model B	model C
β-model	θ_β	-30mV	0	-48.5mV
	ν_β	0.3mV^{-1}	100	1.5mV^{-1}
γ-model	θ_γ	-39mV	-	-
δ-model	θ_δ	-30mV		
	ν_δ	0.3mV^{-1}		
	a	$1ms^{-1}$	-	-
	b	$0.1ms^{-1}$		
all models	E_{in}	-75mV	-1.15	-75mV
	E_{ex}	-10mv	1.15	20mV
	g_0^{in}	1nS	1	5nS
	g_0^{di}	1nS	1	1nS

REFERENCES

[1] A. J. Ijspeert, "Central pattern generators for locomotion control in animals and robots: a review," *Neural Networks*, vol. 21, no. 4, pp. 642–653, 2008.

[2] A. Kozlov, M. Huss, A. Lansner, J. H. Kotaleski, and S. Grillner, "Simple cellular and network control principles govern complex patterns of motor behavior," *Proc. Natl. Acad. Sci. U.S.A.*, vol. 106, no. 47, pp. 20027–20032, 2009.

[3] O. Kiehn, "Decoding the organization of spinal circuits that control locomotion," *Nat. Rev. Neurosc.*, vol. 17, pp. 224–238, 2016.

[4] J. Yu, M. Tan, J. Chen, and J. Zhang, "A survey on CPG-inspired control models and system implementation," *IEEE Trans. Neural Netw. Learn. Syst.*, vol. 25, no. 3, pp. 441–456, March 2014.

[5] L. P. Shilnikov, A. L. Shilnikov, D. V. Turaev, and L. O. Chua, *Methods of qualitative theory in nonlinear dynamics. Volume I*. World Scientific, 1998, vol. 5.

[6] ——, *Methods of qualitative theory in nonlinear dynamics. Volume II*. World Scientific, 2001, vol. 5.

[7] J. Wojcik, J. Schwabedal, R. Clewley, and A. L. Shilnikov, "Key bifurcations of bursting polyrhythms in 3-cell central pattern generators," *PLOS One*, vol. 9, no. 4, p. e92918, 2014.

[8] J. Schwabedal, D. Knapper, and A. Shilnikov, "Qualitative and quantitative stability analysis of penta-rhythmic circuits," *Nonlinearity*, no. 39, p. 3647 – 3676, 2016.

[9] Z. Aminzare, V. Srivastava, and P. Holmes, "Gait transitions in a phase oscillator model of an insect central pattern generator," *SIAM J. Appl. Dyn. Syst.*, vol. 17, no. 1, pp. 626–671, 2018.

[10] A. Sobinov and S. Yakovenko, "Model of a bilateral brown-type central pattern generator for symmetric and asymmetric locomotion," *J. Neurophysiol.*, vol. 119, no. 3, pp. 1071–1083, 2017.

[11] P. Capelli, C. Pivetta, M. S. Esposito, and S. Arber, "Locomotor speed control circuits in the caudal brainstem," *Nature*, vol. 551, no. 7680, p. 373, 2017.

[12] V. Caggiano, R. Leiras, H. Goñi-Erro, D. Masini, C. Bellardita, J. Bouvier, V. Caldeira, G. Fisone, and O. Kiehn, "Midbrain circuits that set locomotor speed and gait selection," *Nature*, vol. 553, pp. 455–460, 2018.

[13] J. Ausborn, N. A. Shevtsova, V. Caggiano, S. M. Danner, and I. A. Rybak, "Computational modeling of brainstem circuits controlling locomotor frequency and gait," *eLife*, vol. 8, 2019.

[14] M. Lodi, A. Shilnikov, and M. Storace, "Design of minimal synthetic circuits with sensory feedback for quadruped locomotion," in *2018 IEEE Int. Symp. Circ. Syst. (ISCAS)*, May 27–30 2018, pp. 1–5.

[15] ——, "CEPAGE: a toolbox for Central Pattern Generator analysis," in *2017 IEEE Int. Symp. Circ. Syst. (ISCAS)*, May 28–31 2017, pp. 1–4.

[16] ——, "Design of synthetic central pattern generators producing desired quadruped gaits," *IEEE Trans. Circuits Syst. I, Reg. Papers*, vol. 65, no. 3, pp. 1028–1039, 2018.

[17] D. A. McCrea and I. A. Rybak, "Organization of mammalian locomotor rhythm and pattern generation," *Brain. Res. Rev.*, vol. 57, no. 1, pp. 134–146, 2008.

[18] N. S. Szczecinski, A. J. Hunt, and R. D. Quinn, "A functional subnetwork approach to designing synthetic nervous systems that control legged robot locomotion," *Front. Neurorobot.*, vol. 11, p. 37, 2017.

[19] X.-J. Wang and J. Rinzel, "Alternating and synchronous rhythms in reciprocally inhibitory model neurons," *Neural Comput.*, vol. 4, no. 1, pp. 84–97, 1992.

[20] E. Marder and R. L. Calabrese, "Principles of rhythmic motor pattern generation," *Physiol. Rev.*, vol. 76, no. 3, pp. 687–717, 1996.

[21] D. Owaki and A. Ishiguro, "A quadruped robot exhibiting spontaneous gait transitions from walking to trotting to galloping," *Sci. Rep.*, vol. 7, no. 1, p. 277, 2017.

[22] J. Ausborn, A. C. Snyder, N. A. Shevtsova, I. A. Rybak, and J. E. Rubin, "State-dependent rhythmogenesis and frequency control in a half-center locomotor cpg," *J. Neurophysiol.*, vol. 119, no. 1, pp. 96–117, 2017.

[23] J. Wojcik, , R. Clewley, and A. L. Shilnikov, "Order parameter for bursting polyrhythms in multifunctional central pattern generators," *Phys. Rev. E*, no. 93, pp. 056 209–6, 2011.

[24] L. Zhao and A. Nogaret, "Experimental observation of multistability and dynamic attractors in silicon central pattern generators," *Phys. Rev. E*, vol. 92, no. 5, p. 052910, 2015.

[25] S. Jalil, D. Allen, J. Youker, and A. Shilnikov, "Toward robust phase-locking in melibe swim central pattern generator models," *Chaos*, vol. 23, no. 4, p. 046105, 2013.

[26] R. Barrio, M. Rodríguez, S. Serrano, and A. Shilnikov, "Mechanism of quasi-periodic lag jitter in bursting rhythms by a neuronal network," *Europhys. Lett.*, vol. 112, no. 3, p. 38002, 2015.

[27] C. Bellardita and O. Kiehn, "Phenotypic characterization of speed-associated gait changes in mice reveals modular organization of locomotor networks," *Curr. Biol.*, vol. 25, no. 11, pp. 1426–1436, 2015.

[28] M. Lemieux, N. Josset, M. Roussel, S. Couraud, and F. Bretzner, "Speed-dependent modulation of the locomotor behavior in adult mice reveals attractor and transitional gaits," *Front. Neurosci.* , vol. 10, p. 42, 2016.

[29] D. H. Perkel and B. Mulloney, "Motor pattern production in reciprocally inhibitory neurons exhibiting postinhibitory rebound," *Science*, vol. 185, no. 4146, pp. 181–183, 1974.

[30] S. M. Danner, S. D. Wilshin, N. A. Shevtsova, and I. A. Rybak, "Central control of interlimb coordination and speed-dependent gait expression in quadrupeds," *J. Physiol.*, vol. 594, no. 23, pp. 6947–6967, 2016.

[31] R. Brette and W. Gerstner, "Adaptive exponential integrate-and-fire model as an effective description of neuronal activity," *J. Neurophysiol.*, vol. 94, no. 5, pp. 3637–3642, 2005.

[32] D. Somers and N. Kopell, "Rapid synchronization through fast threshold modulation," *Biol. Cybern.*, vol. 68, no. 5, pp. 393–407, 1993.

[33] C. Van Vreeswijk, L. Abbott, and G. B. Ermentrout, "When inhibition not excitation synchronizes neural firing," *J. Comput. Neurosci.*, vol. 1, no. 4, pp. 313–321, 1994.

[34] M. Ren, Y. Yoshimura, N. Takada, S. Horibe, and Y. Komatsu, "Specialized inhibitory synaptic actions between nearby neocortical pyramidal neurons," *Science*, vol. 316, no. 5825, pp. 758–761, 2007.

[35] B. W. Connors and S. J. Cruikshank, "Bypassing interneurons: inhibition in neocortex," *Nat. Neurosci.*, vol. 10, no. 7, p. 808, 2007.

[36] A. Sakurai and P. S. Katz, "The central pattern generator underlying swimming in dendronotus iris: a simple half-center network oscillator with a twist," *J. Neurophysiol.*, vol. 116, no. 4, pp. 1728–1742, 2016.

[37] A. Sakurai, C. A. Gunaratne, and P. S. Katz, "Two interconnected kernels of reciprocally inhibitory interneurons underlie alternating left-right swim motor pattern generation in the mollusk melibe leonina," *J. Neurophysiol.*, vol. 112, no. 6, pp. 1317–1328, 2014.

[38] A. Sakurai and P. S. Katz, "Phylogenetic and individual variation in gastropod central pattern generators," *J. Comp. Physiol. A*, vol. 201, no. 9, pp. 829–839, 2015.

[39] A. B. Siddique, L. Pecora, J. D. Hart, and F. Sorrentino, "Symmetry-and input-cluster synchronization in networks," *Phys. Rev. E*, vol. 97, no. 4, p. 042217, 2018.

[40] M. Golubitsky and I. Stewart, "Rigid patterns of synchrony for equilibria and periodic cycles in network dynamics," *Chaos*, vol. 26, no. 9, p. 094803, 2016.

[41] M. Golubitsky, I. Stewart, P.-L. Buono, and J. Collins, "Symmetry in locomotor central pattern generators and animal gaits." *Nature*, vol. 401, no. 6754, pp. 693–695, 1999.

[42] J. Yu, Z. Wu, M. Wang, and M. Tan, "CPG network optimization for a biomimetic robotic fish via pso," *IEEE Trans. Neural Netw. Learn. Syst.*, vol. 27, no. 9, pp. 1962–1968, Sept 2016.

[43] Y. Hu, J. Liang, and T. Wang, "Parameter synthesis of coupled non-linear oscillators for CPG-based robotic locomotion," *IEEE Trans. Ind. Electron.*, vol. 61, no. 11, pp. 6183–6191, 2014.

[44] K. A. Mazurek, B. J. Holinski, D. G. Everaert, V. K. Mushahwar, and R. Etienne-Cummings, "A mixed-signal VLSI system for producing temporally adapting intraspinal microstimulation patterns for locomotion," *IEEE Trans. Biomed. Circuits Syst.*, vol. 10, no. 4, pp. 902–911, 2016.

[45] J. A. Bamford, R. M. Lebel, K. Parseyan, and V. K. Mushahwar, "The fabrication, implantation, and stability of intraspinal microwire arrays in the spinal cord of cat and rat," *IEEE Trans. Neural Syst. Rehabil. Eng.*, vol. 25, no. 3, pp. 287–296, 2017.

[46] S. Jalil, I. Belykh, and A. Shilnikov, "Spikes matter for phase-locked bursting in inhibitory neurons," *Phys. Rev. E*, vol. 85, p. 036214, 2012.

Matteo Lodi was born in Genoa, Italy, in 1991. He received the "Laurea" (M.Sc.) five-year degree (Summa Cum Laude) in Electronic Engineering in 2015 and is currently working towards his Ph.D. degree in Electrical Engineering at the University of Genoa, Italy. He was a visitor in NEURDS-Lab at GSU, Atlanta, USA (2016) and to BioRob Lab at EPFL, Lausanne, Switzerland (2017). His research interests include modeling of nonlinear systems (hysteresis and networks of biological neurons) and bifurcation analysis.

Andrey Shilnikov was born in Nizhny Novgorod, Russia, in 1962. He received M.S. in Mathematics & Physics in 1984, and Ph.D. in Differential Equations incl. Mathematical Physics, in 1990 both from University of Nizhny Novgorod. He was a postdoctoral fellow at UC Berkeley (1993-94), and a Royal Society Postdoctoral Fellow at Cambridge University, UK (1994-1995). Prior to joining GSU in 2000, he held visiting positions at UC Berkeley, Georgia Institute of Technology, and Cornell University. Dr. Shilnikov is GSU Distinguished University Professor at Neuroscience Institute and Department of Mathematics & Statistics. His research interests include dynamical systems and mathematical neuroscience. He is an author of about 100 scholarly publications, including advanced textbooks on dynamical systems. Dr. Shilnikov serves on editorial boards of J. Mathematical Neuroscience, J. Discontinuity, Nonlinearity & Complexity, and J. Frontiers of Applied Mathematics.

Marco Storace (M'01, SM'14) was born in Genoa, Italy, in 1969. He received the "Laurea" (M.Sc.) five-year degree (Summa Cum Laude) in Electronic Engineering in March 1994 and the Ph.D. degree in Electrical Engineering in April 1998, both from the University of Genoa, Italy. Since 2011 he has been a Full Professor in the University of Genoa.He was a visitor to EPFL, Lausanne, Switzerland, in 1998 and 2002. His main research interests are in the area of nonlinear circuit theory and applications, with emphasis on (circuit) models of nonlinear systems (e.g., hysteresis, biological neurons), methods for the piecewise-linear approximation of nonlinear systems, bifurcation analysis and nonlinear dynamics. He is the author or coauthor of about 140 scientific papers, more than an half of which have been published in international journals. He served as Associate Editor of the IEEE TRANSACTIONS ON CIRCUITS AND SYSTEMS – II (2008-2009) and is member of the IEEE Technical Committee on Nonlinear Circuits and Systems (TC-NCAS).